Physical Biology

PAPER

Misalignment between the magnetic dipole moment and the cell axis in the magnetotactic bacterium *Magnetospirillum magneticum* AMB-1

RECEIVED
14 February 2019

REVISED
21 May 2019

ACCEPTED FOR PUBLICATION
10 June 2019

PUBLISHED
18 September 2019

Lucas Le Nagard[1], **Liu Yu**[1], **Murtuza Rajkotwala**[1], **Solomon Barkley**[1], **Dennis A Bazylinski**[2], **Adam P Hitchcock**[3] **and Cécile Fradin**[1,4]

[1] Department of Physics and Astronomy, McMaster University, 1280 Main St. W, Hamilton, ON L8S 4M1, Canada
[2] School of Life Sciences, University of Nevada, 4505 S. Maryland Pkwy, Las Vegas, NV 89154, United States of America
[3] Department of Chemistry and Chemical Biology, McMaster University, 1280 Main St. W, Hamilton, ON L8S 4M1, Canada
[4] Author to whom any correspondence should be addressed.

E-mail: fradin@physics.mcmaster.ca

Keywords: biomagnetism, cell structure, magnetosome, microscopy, cell tracking, magnetotaxis

Supplementary material for this article is available online

Abstract

While most quantitative studies of the motion of magnetotactic bacteria rely on the premise that the cells' magnetic dipole moment is aligned with their direction of motility, this assumption has so far rarely been challenged. Here we use phase contrast microscopy to detect the rotational diffusion of non-motile cells of *Magnetospirillum magneticum* AMB-1 around their magnetic moment, showing that in this species the magnetic dipole moment is, in fact, not exactly aligned with the cell body axis. From the cell rotational trajectories, we are able to infer the misalignment between cell magnetic moment and body axis with a precision of better than 1°, showing that it is, on average, 6°, and can be as high as 20°. We propose a method to correct for this misalignment, and perform a non-biased measurement of the magnetic moment of single cells based on the analysis of their orientation distribution. Using this correction, we show that magnetic moment strongly correlates with cell length. The existence of a range of misalignments between magnetic moment and cell axis in a population implies that the orientation and trajectories of magnetotactic bacteria placed in external magnetic fields is more complex than generally assumed, and might show some important cell-to-cell differences.

1. Introduction

Originally discovered by Bellini [1] in 1963, and later independently re-discovered by Blakemore [2], magnetotactic bacteria (MTB) are motile, Gram-negative prokaryotes ubiquitous in freshwater and marine habitats [3]. They are characterized by their ability to produce magnetosomes, i.e. single magnetic domain crystals of either magnetite (Fe_3O_4) or greigite (Fe_3S_4) surrounded by a phospholipid bilayer [4]. These organelles confer a permanent magnetic moment to MTB, which as a result act as self-propelled micro-compasses swimming along magnetic field lines, presumably in search of favorable growth conditions [5, 6]. Amongst the most thoroughly studied MTB species are strains MS-1 [7], MSR-1 [8], and AMB-1 [9], which belong to the genus *Magnetospirillum*, and all possess a similar helical morphology, with a polar flagellum at each end of the cell [10]. A rigid bundle of protein filaments, formed by the actin-like protein MamK and extending across the cell, serves as a linear scaffold along which the magnetosomes of magnetotactic spirilla are assembled into a chain [11–14].

High resolution methods such as transmission electron microscopy (TEM), that allow for a direct visualization of the magnetosome chain, have shown that in magnetic spirilla, the magnetosome chain is more or less aligned with the helical axis of the cell body [15–17]. By extension, a perfect alignment of the cells' magnetic dipole moment with their long axis (when it exists), and more generally with their swimming direction, is usually taken for granted in all MTB species (with some notable exceptions [18–21]). However, when it comes to a precise determination of the orientation of the magnetic moment, deformations induced

during TEM sample preparation are a possible drawback. In addition, TEM does not provide the direction of the magnetization in individual magnetosomes, which makes it difficult to establish the orientation of the magnetic moment for magnetosome chains with imperfect linear geometries, which are often observed [13, 22, 23].

A precise determination of the alignment between the magnetic moment and the swimming direction is important when trying to interpret distributions of orientations or trajectories of MTB in a magnetic field. In particular, the accuracy of magnetic moment measurements based on cell trajectories or orientation distributions heavily depends on the validity of equating cell direction with the direction of the magnetic dipole moment [24–27]. Although cells of MTB certainly approximately follow magnetic field lines, their alignment with the magnetic field direction is not perfect, and the contribution of thermal noise is often hard to disentangle from other effects, especially for live cells [27, 28]. A misalignment between the magnetic dipole moment and swimming direction can be expected to cause MTB to rotate around the magnetic field lines in helical trajectories, and to broaden the orientation distribution. Helical trajectories have indeed been observed for a few species, a strong hint that magnetic moment and cell axis are not exactly aligned, at least for some MTB [18–21, 24, 29, 30].

In this work, we investigate the possibility of a misalignment between the cell magnetic moment ($\vec{\mu}$) and the cell body axis ($\vec{L}$), and we ask how this may affect the alignment of the cell with an external magnetic field (figure 1). We show that cells with misaligned $\vec{\mu}$ may have a double-peaked orientation distribution as a result of cell body rotation around $\vec{\mu}$, and we use phase microscopy to test this prediction in cells of *Magnetospirillum magneticum* strain AMB-1. We take advantage of the helical shape of spirilla, which allows for the determination of both the projection of $\vec{L}$ in the focal plane and the cell body rotation around $\vec{L}$, to show that most cells do visibly rotate around $\vec{\mu}$, proving that $\vec{\mu}$ is not perfectly aligned with $\vec{L}$. Finally, we demonstrate that taking into account the misalignment between cell magnetic moment and cell axis allows using the cell orientation distribution to perform a precise measurement of its magnetic moment.

2. Theory: distribution of orientations for a MTB placed in a uniform magnetic field

In this section, we derive the orientation distribution of a MTB placed in a constant uniform magnetic field ($\vec{B}$). In most previous works, the magnetosome chain and the permanent magnetic dipole moment of the MTB ($\vec{\mu}$) are presumed to be aligned with the long axis of the cell body ($\vec{L}$). In contrast, the theory we develop here takes into account a possible misalignment between cell body axis and cell magnetic dipole moment. This is illustrated in figure 1, which shows a magnetotactic spirillum with a non-zero inclination, β, between $\vec{\mu}$ and $\vec{L}$.

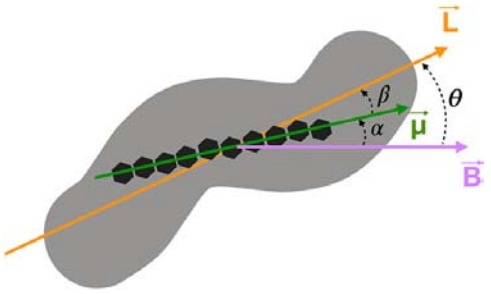

Figure 1. Schematic representation of a magnetotactic spirillum placed in a uniform magnetic field ($\vec{B}$), and presenting a misalignment (β) between the cell long axis ($\vec{L}$, defined here as the axis of the helical cell body) and the cell permanent magnetic moment ($\vec{\mu}$, considered here to be aligned with the magnetosome chain). The magnetic energy of the system depends on the angle α between $\vec{\mu}$ and $\vec{B}$, whereas θ is the apparent cell orientation with respect to the magnetic field. Although all three vectors ($\vec{L}$, $\vec{\mu}$ and $\vec{B}$) are represented here in the same plane for simplicity, it does not in general have to be the case.

When observing spirilla using phase microscopy, two angles related to cell orientation (θ, ψ) can be determined from the projected shape of the cell in the focal plane (figure 2(a)). θ is the apparent orientation of the cell axis with respect to the magnetic field direction (chosen here to be horizontal), i.e. the angle between $\vec{B}$ and the horizontal projection of $\vec{L}$. ψ is the angle describing the rotation of the cell around its helical axis. Our goal is thus to calculate the probability of finding the cell in a certain orientation, $p(\theta, \psi)$, a quantity that we can access experimentally, and to see how this probability is modified when $\vec{\mu}$ and $\vec{L}$ are misaligned.

2.1. Influence of thermal motions

We first consider the simple case, discussed previously in several publications, where the magnetic moment is aligned with the cell axis ($\beta = 0$), and fluctuations in the orientation of $\vec{\mu}$ relative to $\vec{B}$ (fluctuations in the value of α) are due to thermal noise [3, 15, 27, 31]. The orientation of the cell in three dimensions is fully characterized by three angles (θ, η, ψ), defined in figure 3(a). θ is the azimuthal angle, and also represents the (experimentally accessible) apparent orientation of the cell in the focal plane. η is the inclination of the cells with respect to the optical axis. ψ describes the rotation of the cell body around the long axis of the cell. The orientation of the cell in an external magnetic field is described by Boltzmann statistics, similarly to that of spins in a paramagnetic material. The magnetic energy of the system depends on the relative orientation of $\vec{\mu}$ and $\vec{B}$: $E(\alpha) = -\vec{\mu}.\vec{B} = -\mu B \cos\alpha = -\mu B \sin\eta \cos\theta$. The probability density associated with a certain orientation is therefore:

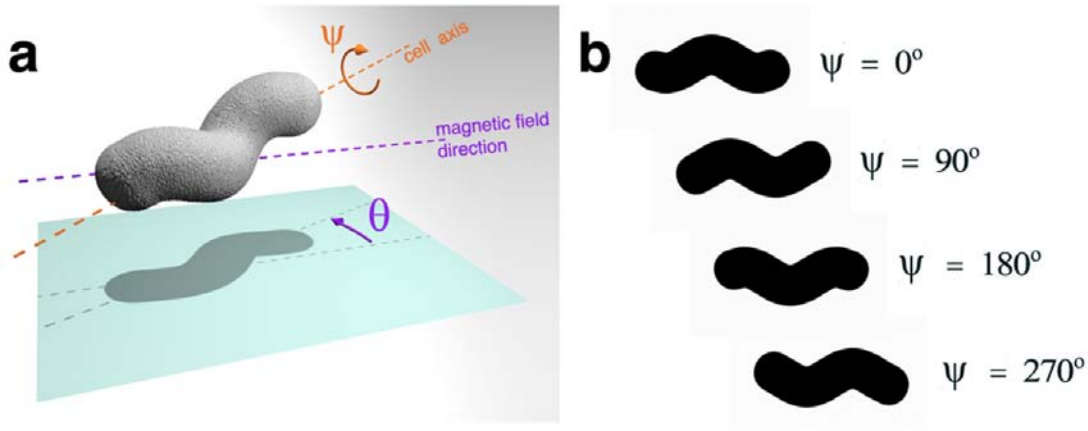

Figure 2. (a) Three-dimensional representation of a helical cell, showing the two angles that can be determined using phase microscopy, the apparent cell orientation in the focal plane, θ, and the rotation of the cell body around the helical cell axis, ψ. The dashed purple line represents the direction of the magnetic field, $\vec{B}$, while the dashed orange line represents the direction of the cell axis, $\vec{L}$. (b) Projection of the cell in the focal plane for different rotations of the cell body around its helical axis.

$$p_{T,3D}(\theta,\eta) = \frac{R}{4\pi \sinh(R)} e^{R \sin\eta \cos\theta}, \quad (1)$$

where we have introduced the quantity $R = \mu B/kT$ (T is the absolute temperature in Kelvin), which describes the balance between magnetic and thermal energy. The probability to observe a particular cellular orientation θ in the focal plane can be calculated by integrating equation (1) over all possible values of η:

$$p_T(\theta) = \frac{R}{4\sinh(R)} \left[L_{-1}(R\cos\theta) + I_1(R\cos\theta)\right], \quad (2)$$

where L_{-1} is the modified Struve function of the first kind of order -1 and I_1 is the modified Bessel function of order 1. Note that in this case, the probability to find the cell body in a certain orientation, $p_T(\theta)$, is decoupled from the rotation of the cell body around its long axis, ψ. This is can be seen in the lower panel of figure 3(a), which illustrates that $p_T(\theta)$ does not depend on ψ.

Instead, $p_T(\theta)$ strongly depends on R. For a typical value of the magnetic moment ($\mu \simeq 10^{-16}$–10^{-15} A $\cdot$ m^2) and a sufficiently high magnetic field ($B \simeq 1$ mT and above), we have $R \gg 1$, which means that magnetic effects dominate over thermal effects. In this case, the orientation of $\vec{\mu}$ is close to that of $\vec{B}$, and as a result close to horizontal. The probability density is then well described by equation (3), which is the orientation distribution obtained for a cell constrained to a two-dimensional motion in the focal plane [27]:

$$p_T(\theta) \simeq \frac{1}{2\pi I_0(R)} e^{R\cos\theta}, \quad (3)$$

where I_0 is the modified Bessel function of order 0.

2.2. Influence of a permanent misalignment between cell magnetic moment and cell body axis

We next consider another limiting case (figure 3(b)), where the magnetic moment is perfectly aligned with the magnetic field ($\alpha = 0$, which is expected in the limit where $R \to \infty$), but where there is a permanent misalignment between magnetic moment and cell body axis ($\beta \neq 0$). Such a misalignment between $\vec{\mu}$ and $\vec{L}$ can for example be expected if the magnetosome chain is not aligned with the cell body axis. The cell can then take any orientation on a cone of aperture 2β (see upper panel of figure 3(b)). As it rotates around this cone, the cell also rotates around its own body axis, such that there is a simple geometrical relationship between ψ and the apparent orientation of the cell body in the focal plane: $\theta(\psi) = \tan^{-1}[\tan\beta \cdot \cos\psi]$. As ψ passes from 0 to 2π, the apparent cell orientation varies between $-\beta$ and β. Taking into account this geometrical constraint, and assuming a uniform distribution for ψ (as expected if the cell rotates freely around its magnetic moment), we find that the probability distribution for the observed cell orientation in the presence of a fixed misalignment between $\vec{\mu}$ and $\vec{L}$ is:

$$p_M(\theta,\psi) = \frac{1}{2\pi}\delta\left(\theta - \tan^{-1}[\tan\beta\cdot\cos\psi]\right), \quad (4)$$

where $\delta(x)$ is the Dirac delta function. The probability distribution for the apparent orientation of the cell with respect to the magnetic field can be calculated in the interval $[-\beta, +\beta]$ by integrating equation (4) over ψ, yielding:

$$p_M(\theta) = \frac{1}{\pi\cos^2\theta}\frac{1}{\sqrt{\tan^2\beta - \tan^2\theta}}. \quad (5)$$

This apparent orientation distribution presents two sharp peaks, at $-\beta$ and $+\beta$ (see the lower right panel of figure 3(b)).

2.3. Combined effects of thermal motions and of a permanent misalignment between magnetic moment and cell body axis

In a real system, we expect both a small constant misalignment between magnetic moment and cell body (non-zero β) and a small fluctuating

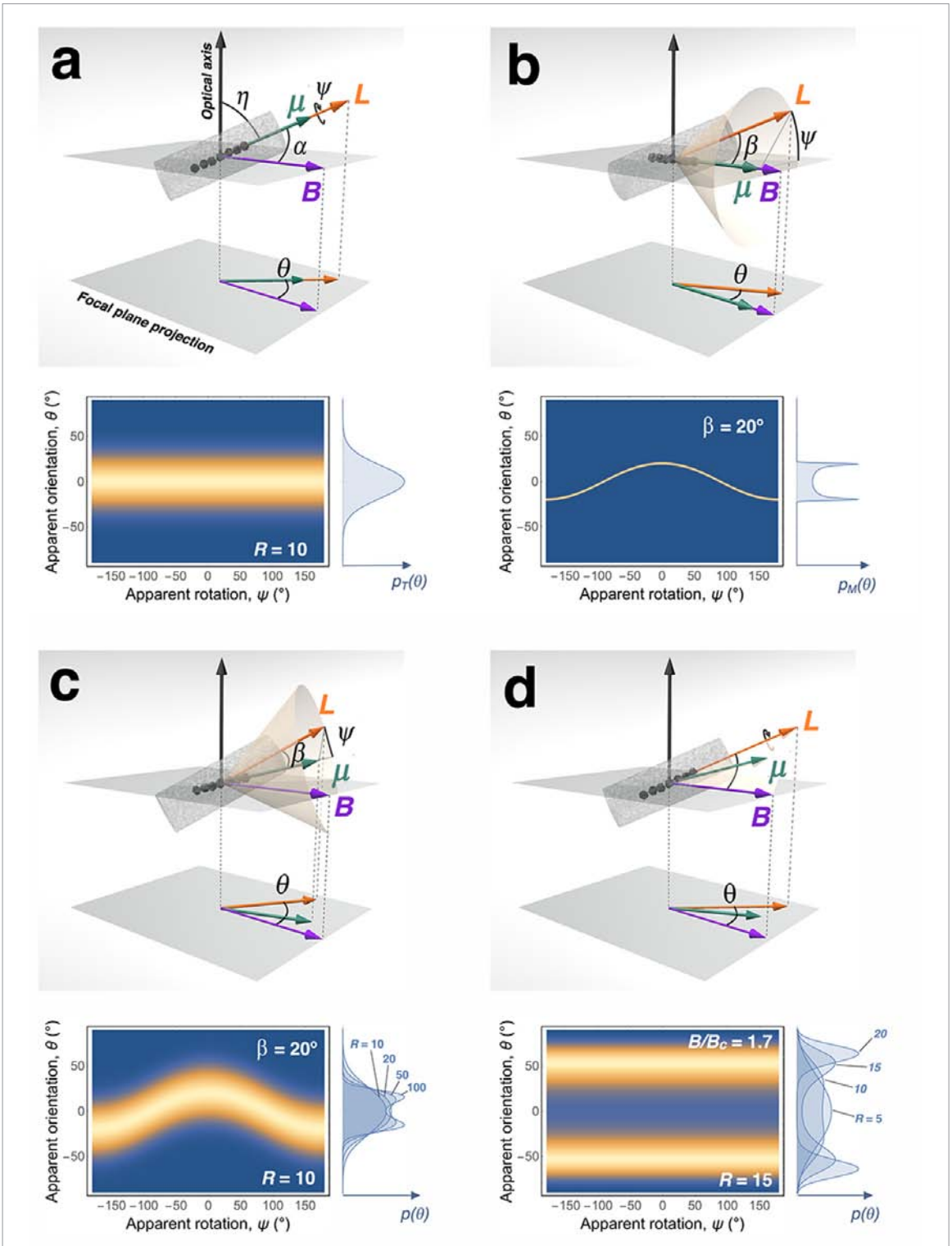

Figure 3. (a) Geometry in the absence of misalignment between $\vec{\mu}$ and $\vec{L}$, but considering fluctuations away from $\vec{B}$ due to thermal noise. (b) Geometry in the presence of a fixed misalignment between $\vec{\mu}$ and $\vec{L}$. In a sufficiently strong magnetic field, $\vec{\mu}$ is aligned with $\vec{B}$ and $\vec{L}$ is rotating on a cone. For small misalignments, the angle characterizing the rotation of the cell on this cone can be equated to ψ. (c) Geometry in the presence of both a fixed misalignment between $\vec{\mu}$ and $\vec{L}$ and thermal fluctuations. (d) Geometry in the presence of thermal fluctuations and a varying misalignment between $\vec{\mu}$ and $\vec{L}$ due to the magnetic susceptibility anisotropy of the magnetosome chain. Note that in this case $\vec{\mu}$ is always found in the plane defined by $\vec{B}$ and $\vec{L}$. For each different geometry, the expected distribution of orientations, $p(\theta, \psi)$, is shown in a density plot placed in the lower part of the panel, and the integrated distribution, $p(\theta)$, is shown on the right side of the density plot.

misalignment between magnetic moment and magnetic field due to thermal motions (non-zero α), as depicted in figures 1(a) and 3(c). As long as these angles remain small ($\alpha, \beta < 20°$), we can consider that these two effects are independent of each other, such that the apparent orientation distribution of the cell can be obtained by convoluting the probability distributions in equations (3) and (4):

$$p(\theta,\psi) \simeq \int_{\theta-\beta}^{\theta+\beta} p_T(\chi)\, p_M(\theta-\chi,\psi)\, d\chi. \quad (6)$$

This can be solved to yield:

$$p(\theta,\psi) \simeq \frac{1}{(2\pi)^2 I_0(R)} e^{R\cos\left[\theta-\tan^{-1}[\tan\beta\cdot\cos\psi]\right]}. \quad (7)$$

In such cases, the probability distribution $p(\theta,\psi)$ has a distinctive pattern, which is shown in the lower panel of figure 3(c). It combines features of both $p_T(\theta)$ and $p_M(\theta,\psi)$. Most striking is the characteristic sine-like dependence between θ and ψ, a result of the constraint existing between rotation of the cell around its magnetic moment and rotation around its body axis.

Equation (7) can be integrated numerically over ψ to find the apparent angle distribution $p(\theta)$ (shown in the lower right panel of figure 3(c)). This distribution changes systematically with the value of β. At low values of β it has a single central peak, which changes to two peaks symmetric about the origin at high values of β. These peaks are positioned just above $-\beta$ and just below $+\beta$. The higher the value of R (the larger the magnetic effects compared to the thermal effects), the sharper the peaks. However, the positions of the peaks remain unchanged as they are set by β, the value of the misalignment.

2.4. Influence of an induced misalignment between $\vec{\mu}$ and $\vec{L}$ due to magnetic susceptibility anisotropy of the magnetosome chain

We finally consider a cell whose magnetosome chain is aligned with the cell axis, but which has a non-zero magnetic susceptibility perpendicular to this axis. While the concept of magnetic susceptibility is often discussed in the context of a single particle or crystal, here we apply it to the magnetosome chain as a whole. In this case, magnetic susceptibility may originate both from changes in the magnetization of the individual magnetosomes (due to rotation of the spins towards the magnetic field direction) and from changes in the orientation and organization of these magnetosomes (which in the context of the cell are at least partially constrained by attachment to the MamK filament bundle). The magnetic susceptibility of magnetosome chains in aligned frozen bacteria was found to be non-zero, both parallel and perpendicular to the magnetosome chain [23].

The magnetic moment of a susceptible material (here the magnetosome chain as a whole) will acquire a small component perpendicular to the chain axis when it is placed in a magnetic field ($\mu_\perp = \chi_\perp B \sin\alpha$ at small field). The magnetic moment component along the chain axis also changes, to $\mu + \chi_\parallel B\cos\alpha$ at small field, where μ is the value of the remanent magnetic moment at $B = 0$. This leads to a change in the direction of the magnetic moment away from the magnetosome axis (and and in effect a misalignment between the magnetic moment and the cell axis), and towards the magnetic field (figure 3(d)). The magnetic susceptibility affects the magnetic potential energy, and an anisotropy, $\Delta\chi = \chi_\parallel - \chi_\perp$, between its components parallel ($\chi_\parallel$) and perpendicular ($\chi_\perp$) to the magnetosome chain affect the dependence of this energy on the orientation of the magnetosome chain in the magnetic field (α) [32]:

$$E(\alpha) = -\mu B\cos\alpha - \frac{V\Delta\chi B^2\cos^2\alpha}{2\mu_0}. \quad (8)$$

Here V is the volume of the magnetosome chain and μ_0 is the vacuum permeability. Only terms with an explicit dependence on α are included in equation (8) (as the value of B is fixed in our experiments). The first term in equation (8) describes the interaction between the applied magnetic field and the permanent magnetic moment, while the second term describes the interaction of that magnetic field with the induced magnetic moment. The presence of the quadratic term, B^2, in equation (8) implies that, for $\Delta\chi < 0$, there is a critical field value $B_c = -\mu_0\mu/(V\Delta\chi)$. For $B > B_c$ the energy minimum is no longer found at $\alpha = 0$ (where the cell tends to align with the magnetic field), but instead at $\alpha_c = \cos^{-1}[B_c/B]$ (where the cell tends to lie at an angle α_c from the direction of the magnetic field). However, contrary to the previous case, the direction of $\vec{\mu}$ is not coupled with the rotation of the cell around its main axis (i.e. with the value of ψ). Instead $\vec{\mu}$ always lies in the plane defined by $\vec{L}$ and $\vec{B}$.

As in the simple case considered in section 2.1, we assume that thermal motions can be assimilated into the distribution as if motions were restricted to the focal plane, which is justified for large R. In this case the combination of magnetic susceptibility anisotropy of the magnetosome chain and thermal motions of the cell leads to the following equation for the cell orientation distribution in the focal plane:

$$P(\theta) = e^{R\left(\cos\theta - \frac{1}{2}\frac{B}{B_c}\cos^2\theta\right)}/\mathcal{Z}, \quad (9)$$

with the partition function:

$$\mathcal{Z} = \int_{-\pi}^{\pi} e^{R\left(\cos\theta - \frac{1}{2}\frac{B}{B_c}\cos^2\theta\right)} d\theta. \quad (10)$$

As in the case of a permanent misalignment between $\vec{\mu}$ and $\vec{L}$, the orientation distribution has two symmetric peaks, whose width varies with R (lower right panel in figure 3(d)). However, in contrast with the fixed misalignment case, the position of these peaks depends on the magnitude of the field. Also, in stark contrast with the previous case, the apparent orientation of the cell, θ, does not depend on ψ.

3. Methods

3.1. AMB-1 cultures

Cells of *Magnetospirillum magneticum* strain AMB-1 were grown in liquid medium under heterotrophic conditions, in a growth medium containing, per liter: 1.0 ml modified Wolfe's mineral elixir [33, 34], 0.1 g

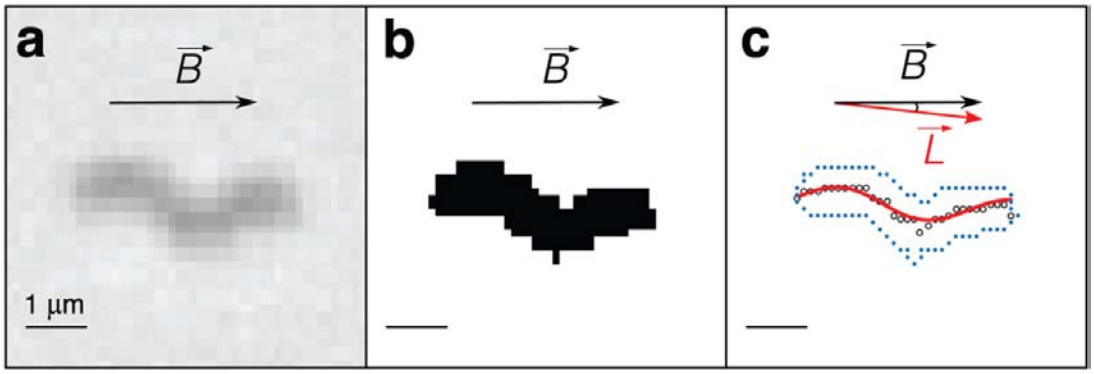

Figure 4. Analysis of optical microscopy movies. (a) Original phase contrast microscopy image. (b) Binarized image used to perform the sine fit. (c) Image obtained after the sine fit analysis, displaying the edges of the cell (blue dots), the cell backbone (black circles) and the fitted sine function (red line). Black arrows: magnetic field direction. Red arrow: cell orientation in the focal plane, measured from the sine fit. Scale bars: 1 μm

KH_2PO_4, 0.15 g $MgSO_4{\cdot}7H_2O$, 2.38 g HEPES, 0.34 g $NaNO_3$, 0.1 g yeast extract, 3.0 g BD Bacto Soytone, 4.35 ml potassium lactate (60% solution) and 5 ml Fe (III) citrate 10 mM solution. The pH was adjusted to 7.0 and dissolved O_2 was removed by bubbling N_2 in the medium. Bacteria were grown in 125 ml sealed glass bottles containing 60 ml of growth medium. Air in the headspace of the culture flasks was first replaced by N_2, then 1 ml O_2 was added in the headspace before inoculation (to reach 1.5% volume concentration of O_2 in the headspace) [35].

3.2. Optical microscopy

3.2.1. Sample preparation

Cells were harvested 3 to 6 days after inoculation and immediately killed by heating at 50°C for 15 min (using dead cells allowed studying their thermal motions in the absence of biological noise). The bacterial suspension was then promptly diluted with fresh medium (1:10 dilution) and injected into custom-made observation chambers for immediate observation (as over time some cells may stick on the chamber surfaces). The chambers were made of a glass slide and a coverslip separated by two melted parafilm spacers, creating a channel of approximately 1 cm in length, 5 mm in width and 100–200 μm in height. The channels were sealed with vacuum grease to avoid evaporation.

3.2.2. Data collection

Samples were studied with an upright microscope (Nikon Eclipse E200-LED) using a 40× phase contrast objective. The stage of the microscope was modified to install two custom-made electromagnetic coils (3.6 cm in diameter, 4 cm coil spacing, copper wire, 300 loops per coil) reinforced by two iron cores. Constant magnetic fields parallel to the focal plane were applied by circulating a current through the coils, using an Agilent 33120A power supply connected to an Agilent 33502A amplifier. Movies of dead bacteria in constant fields (1.0 and 1.9 mT) were acquired with a Prosilica GE (Allied Vision) camera at 100 frames per second. The average movie duration was 30 s, with no movie shorter than 15 s.

3.2.3. Data analysis

A code was written in MATLAB R2016a to determine the cell morphology and orientation from binarized microscopy images using a sine fit (as illustrated in figure 4). For each frame of the recorded movies, the binarized image of the cell was first translated to the origin and a first approximation of its orientation was obtained by fitting the cell body (treated as a cloud of points, each one of them at the centre of one of the black pixels obtained from the binarization step) to a straight line. The cell was then rotated by the corresponding angle to make it approximately horizontal. Pixels were binned vertically to obtain a line corresponding to the cell backbone, and this line was then fitted by a sine function. These two steps (rotation and sine fitting) were repeated 16 more times for each cell, for rotation angles covering a $\pm$ 8° interval around the angle obtained with the line fit (1° steps). The angle leading to the minimum error in the sine fit was recorded and two additional angles were tested around it, respectively at $-0.5°$ and $+0.5°$. The angle corresponding to the minimum error after that last step was recorded as the cell orientation, and other parameters of interest (phase ϕ and amplitude of the sine function, length of the cell) were also saved, for each frame. A similar strategy has previously been used by Constantino *et al* to measure the orientation of another helical bacteria, *Helicobacter pylori* [36]. Because all measurements were done here in the presence of a magnetic field tending to keep the cell body in the focal plane, the length of the cell was later simply estimated as the average length over all frames.

For a cell with a helical shape whose direction is close to horizontal, the projection of the cell body in the focal plane has a sinusoidal shape. The phase of this sinusoidal shape, ϕ, is directly related to the rotation of the cell around the helical axis, ψ (as illustrated in figure 2). One has: $\psi = \phi + \delta$, where δ is a geometrical phase shift whose value only depends on cell geometry

and is thus constant for a particular cell. In the end, it follows from equation (4) that, if the angle between the cell magnetic moment and its main axis is β, then the following relationship should be expected between ϕ and θ (two quantities which are experimentally accessible with phase microscopy):

$$\theta(\phi) = \tan^{-1}\left(\tan\beta \cdot \cos(\phi + \delta)\right). \quad (11)$$

The error on the values of the angles θ and ψ was evaluated by comparing measurements of these angles for the same cell in successive frames. Because the cell has very little time to change orientation in the 10 ms separating two consecutive frames, the difference in the obtained values of θ and ψ is primarily due to measurement error. For θ, an estimate of this experimental error is then obtained by calculating the standard deviation of that difference:

$$\sigma = \sqrt{\frac{1}{N}\sum_{i=1}^{N}(\theta_{i+1} - \theta_i)^2}, \quad (12)$$

where θ_i is the value of θ measured in frame i. The error on ψ can be estimated in the same way. We find that the precision on the measurement of θ is on the order of or better than 3°, while the precision on the measurement of ψ is on the order of or better than 15°.

3.2.4. *Orientation distribution analysis*

All experimentally measured orientation distributions were plotted as histograms, with a bin width of 2°. They were then compared to the distribution expected in the small angle limit for simple Boltzmann statistics (equation (3)), by using discrete Boltzmann statistics, in which case an excellent approximation for equation (3) is given by:

$$p(\theta_n) = e^{R\cos\theta_n}/\mathcal{Z}, \text{ with } \mathcal{Z} = \sum_{\theta_i} e^{R\cos\theta_i}. \quad (13)$$

Fit of experimental distributions with equation (13) allows extracting a value for $R = \mu B/kT$, from which μ can then be calculated.

3.3. Transmission electron microscopy (TEM)

Samples were prepared by deposition and subsequent drying in air at room temperature of a droplet of growth medium onto a formvar-coated TEM grid. Unstained bacteria were imaged using a JEOL 1200EX TEMSCAN microscope. To estimate the orientation of the magnetic moment of individual cells, the magnetosome chain was divided into short segments. The orientation of each segment was determined through linear least square fitting and the volume of magnetic material in each segment was estimated by assuming a spherical shape for the magnetosomes. The orientation of the total magnetic dipole moment was determined by computing the volume-weighted average orientation of all segments. The orientation of the cell body was measured using the sine fit method described above.

3.4. Scanning transmission x-ray microscopy (STXM)

Samples were prepared exactly as for TEM. STXM measurements were done at the HERMES beamline (SOLEIL synchrotron) using a 40 nm outer zone Fresnel zone plate, by measuring a stack of images at the Fe L_3 edge (704–717 eV) with right circularly polarized (RCP) x-rays. No magnetic field was applied, thus the magnetosome chains were in their remanent state. Data analysis was performed using aXis2000 (09-Oct-2016 version) [37]. The Fe L_3 edge absorption spectrum of a magnetosome depends on the orientation of its magnetic moment with respect to the direction of propagation of the RCP light. Comparison to a reference spectrum for magnetite [38] therefore allows to determine the relative direction of magnetization of each subchain in a magnetosome chain. The difference in optical density (DOD) between the two types of subchains is equivalent to the x-ray magnetic circular dichroism (XMCD) spectrum for magnetite.

4. Results

In order to test the plausibility of a misalignment between the cell axis ($\vec{L}$) and the magnetic moment ($\vec{\mu}$) in cells of AMB-1, we first imaged 50 cells with electron microscopy. For each of these cells we estimated the direction of $\vec{L}$ based on cell shape, and the direction of $\vec{\mu}$ based on the morphology of the magnetosome chain, by making the assumption that the magnetic moment of each linear subchain in the magnetosome chain was aligned with the subchain axis and proportional to the amount of magnetic material in the subchain (see figure 5 and section 3.3). This analysis suggests that, for a significant number of cells, the direction of the magnetic moment differed from that of the cell body axis. We found that for the studied population there is an average difference of 6° between magnetic moment direction (as estimated from magnetosome chain geometry) and cell body axis, with a large standard deviation $\sigma = 6°$. We also estimated the average saturation magnetic moment (μ_{sat}) of each cell by multiplying the average volume of magnetite per cell by the saturation magnetization of magnetite, M_{sat} [27, 39]. Using $M_{sat} = 4.8 \times 10^{-22}$ A · m^2 · nm^{-3} [40], we obtained $\mu_{sat} = (12 \pm 4) \times 10^{-16}$ A · m^2 (mean ± standard deviation), with an average number of magnetosomes per cell equal to 30 ± 7. The remanent magnetic moment (estimated to be 80% –90% of the saturation magnetic moment for aligned MTB [41, 42] and for linear assemblies of magnetite particles extracted from MTB [43]) for cells in this population is thus on average $\mu \simeq 10 \times 10^{-16}$ A · m^2.

An important assumption made when determining the direction of the magnetic moment and the value of μ_{sat} from TEM images is that all segments in the magnetosome chain have their magnetic moments pointing in the same overall direction along the magnetosome chain (something which is strongly suggested

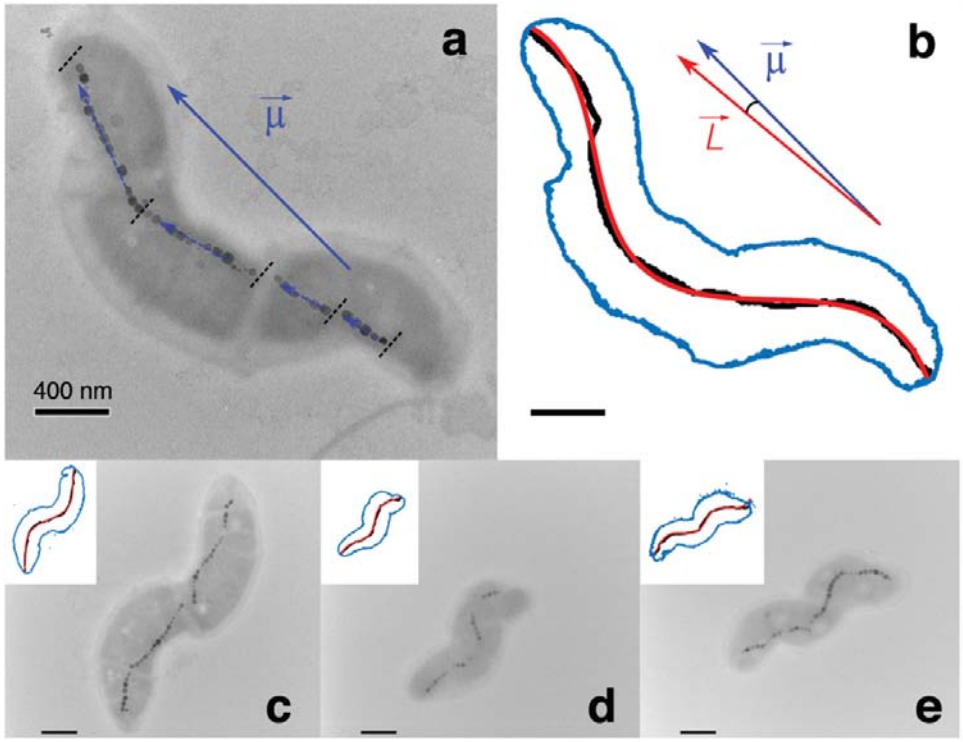

Figure 5. TEM images of cells of *Magnetospirillum magneticum* strain AMB-1 that suggest there is a small structural misalignment between the cell body axis and the magnetosome chain, and assuming that magnetic moment is aligned with the magnetosome chain, that there is therefore a misalignment between cell magnetic moment and cell body axis. (a) The magnetic moment orientation of the cell (blue arrow) is determined by adding the contributions of each of the magnetosome subchains (dashed blue arrows). (b) The cell axis is determined by approximating the cell backbone to a sine function, as illustrated here for the cell shown in (a). The edges of the cell are shown in blue, the backbone obtained by binning the pixels constituting the cell in black, and the sinusoidal function fitted to the backbone in red. The misalignment between cell axis (red arrow) and chain axis (blue arrow) was $\beta = 5.2°$ in this case. ((c)–(e)) Additional examples of AMB-1 cells with different degrees of misalignment (11.2°,1.2° and 0.6°, respectively). Corresponding sine fit analysis are shown in the insets. Scale bars: 400 nm.

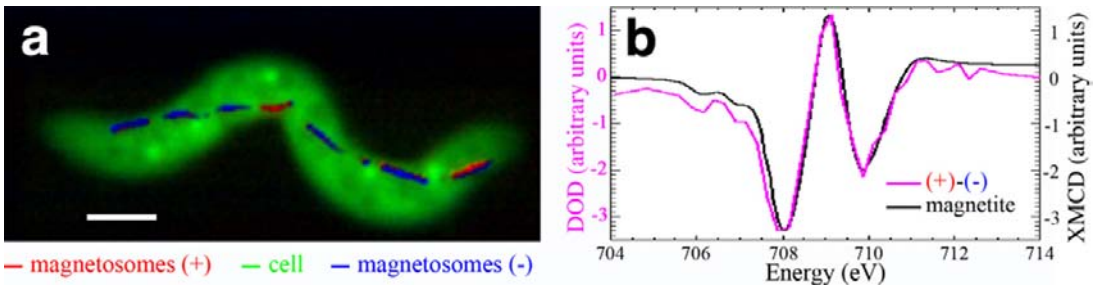

Figure 6. STXM of an AMB-1 cell (no applied magnetic field). (a) Three-component false color map showing the regions of the sample associated with the three principal absorption spectra observed in this sample: the cell (green), and magnetosome subchains with opposite polarities (blue, red). Scale bar: 500 nm. (b) Difference in optical density (DOD) spectrum obtained by subtracting the average blue magnetosome absorption spectrum from the average red magnetosome absorption spectrum, compared to the reference x-ray magnetic circular dichroism (XMCD) signal of magnetite [38].

by off-axis electron holography studies done on strains closely related to AMB-1, MS-1 and MV-1 [44, 45]). However, AMB-1 cells often present a magnetosome chain fragmented into subchains separated by gaps. Thus opposite magnetic polarities between subchains are possible, as has been previously observed in cells of another helical- to comma-shaped MTB, *Magnetovibrio blakemorei* strain MV-1 [46]. We indeed observed this phenomenon in some cells of AMB-1 imaged with STXM, using right circularly polarized x-rays (figure 6). Magnetosome chains with opposite polarities are clearly visible in the three-component false-color composite image of the cell shown in figure 6(a). The difference between the absorption spectra of chains rendered in red and that of those rendered in blue is shown in figure 6(b). It is in agreement with the reference x-ray magnetic circular dichroism (XMCD) signal of magnetite [38]. This confirms that blue and red subchains have opposite polarities. We did not investigate the frequency of these opposite magnetic polarities in magnetosome subchains in AMB-1, but this finding is consistent with previous results from

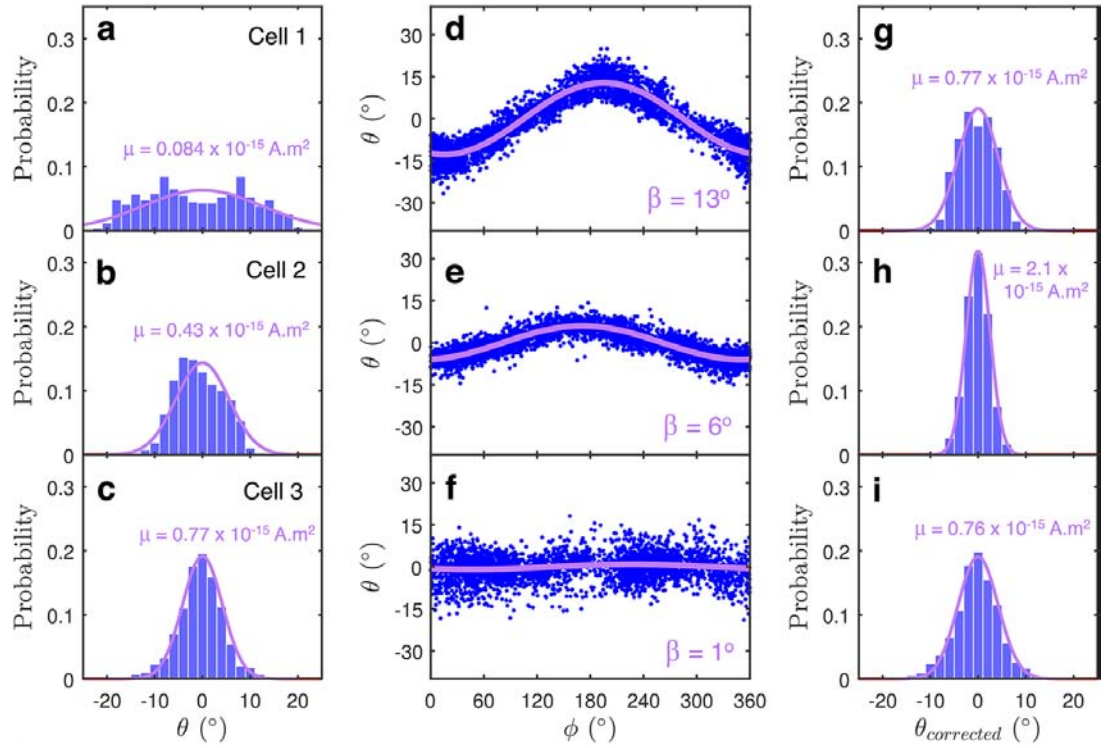

Figure 7. Measurement and correction of the misalignment for three representative cells placed in a constant 1.0 mT magnetic field. ((a)–(c)) Experimental orientation distributions. Equation (13) does not always provide a good fit to these distributions (solid purple line, the values of μ obtained from the fits are indicated for each cell). ((d)–(f)) Relationship between θ and ϕ. Equation (11) provides a good fit to the experimental data (solid purple line). The value of the misalignments provided by this fit is indicated on the figure for each cell. ((g)–(i)) Corrected orientation distributions obtained after subtraction of the phase-dependent artefact caused by the misalignment. Equation (13) (solid purple line) now always provides a good fit to these corrected histograms (the obtained value of μ is indicated on the figure for each cell).

cells of *Magnetovibrio blakemorei* strain MV-1 where $4.0\% \pm 0.2\%$ of cells had magnetosome subchains with opposing magnetic orientations [46].

Although TEM images do suggest that there is a misalignment between cell body axis and magnetic moment, the possible alteration of the cell morphology upon drying of the TEM samples, along with the possible presence of magnetic reversals, cast a doubt on how accurately this misalignment can be measured by TEM. To more precisely and confidently measure the misalignment between the magnetic moment and cell body axis, we imaged 111 non-motile cells placed in a constant magnetic field ($B = 1.0$ mT) using optical phase microscopy. For each cell and for each image of this cell in the recorded movie, the apparent orientation of the cell in the focal plane and its rotation around its body axis were determined, using the sine fit method detailed in the Methods (section 3.2). The orientation distributions of three typical cells are presented in figures 7(a)–(c). In cases (a) and (b), the discrepancy between the orientation distribution and the expected Boltzmann distribution is quite evident, with the experimental distribution clearly displaying two symmetric peaks in (a). As shown in the Theory section (section 2), such an effect is expected either if there is a permanent misalignment between the magnetic dipole moment and cell axis or if the magnetosome chain has a significant magnetic susceptibility anisotropy. This second possibility is suggested by magnetic susceptibility measurements, performed on either aligned chains of magnetosome particles or frozen aligned cells, which show that the magnetic susceptibility of the chains at low magnetic field is greater in the direction perpendicular to the chain than in the parallel direction [23, 43]. To distinguish between these two scenarios, the apparent orientation of the cell with respect to the magnetic field direction, θ, was plotted as a function of its rotation around the cell axis, ϕ, for each cell. In all cases, the relationship observed between θ and ϕ was consistent with the behaviour predicted by equations (7) and (11) derived assuming the existence of a small permanent misalignment between $\vec{\mu}$ and $\vec{L}$ (figures 7(d)–(f)). This strongly suggests that the misalignment observed between $\vec{B}$ and $\vec{L}$ is due to a permanent misalignment between magnetic moment and cell axis (as also suggested by the TEM measurements), as opposed to magnetic susceptibility anisotropy of the magnetosome chain. Using equation (11) to fit the experimentally established relationship between θ and ϕ allowed us to precisely measure the misalignment β for each cell (figures 7(g)–(i)).

As seen in section 2.3, the existence of a misalignment of the magnetic moment broadens the orientation distribution and can lead to two-peaked distributions in extreme cases (as observed for example in figure 7(a)). This in turn affects the value of the

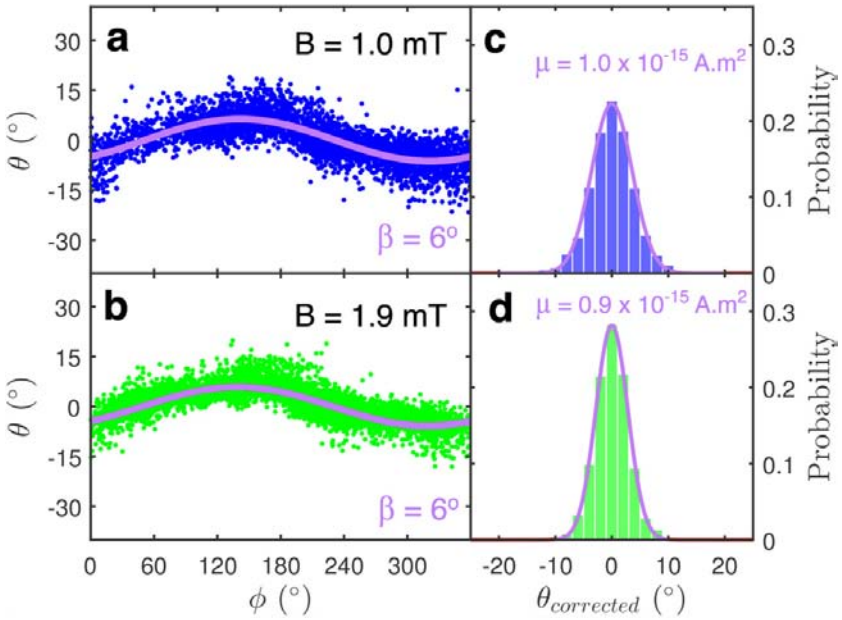

Figure 8. Magnetic moment measurement for the same cell at two different magnetic field strengths. ((a) and (b)) Relationship between θ and ϕ obtained at 1.0 mT (a) and 1.9 mT (b). Equation (11) fitted to experimental data returns as expected the same misalignment $\beta = 6°$ in both cases. ((c) and (d)) Corrected histograms obtained by subtracting equation (11) to the data and then subtracting the mean value ($-0.1°$ for (c) and $0.5°$ for (d)) to centre the histograms. Equation (13) was fitted to these corrected histograms (solid purple line) and returns as expected similar values of μ for both fields (indicated on the figure).

magnetic moment obtained by fitting the orientation distribution with standard Boltzmann statistics. In the small angle limit, the effects of thermal noise and misalignment add up. Orientation distributions can thus be corrected by subtracting the best fit line obtained with equation (11) (purple line in figures 7(d)–(f)) to the experimental value of $\theta(\phi)$ (blue symbols in the same figures). The corrected distributions are governed by thermal fluctuations only, and can thus be fitted with equation (13) to measure μ (figures 7(g)–(i)). The values of μ obtained after data correction are, as expected, generally higher than before correction, and sometimes very significantly higher when β is large. To assess the error on β and μ measured in this way, the data was split into 5 separate subsets of data for each of the three cells presented in figure 7. The misalignment and corrected magnetic moment were measured for each subset, and the error was recorded as the standard deviation of these 5 measurements (see supplemental (stacks.iop.org/PhysBio/16/066008/mmedia)). Typical error on β is 0.5°. The error on μ generally varied between 10% and 20%.

In order to further confirm that the observed orientation distributions are explained by a small permanent misalignment of the magnetic moment with respect to the cell axis, we studied several cells of AMB-1 at two different magnetic field strengths. Representative results obtained for one cell are presented in figure 8. The same misalignment was measured and similar values of the magnetic moment were obtained after correcting for this misalignment, confirming that any eventual anisotropy of magnetic susceptibility of the magnetosome chain can be neglected for the values of the field tested in this work. In addition, it demonstrates that the contribution of the misalignment to the orientation distributions is effectively corrected by subtracting equation (11).

We observed a positive correlation between L and μ (figures 9(a) and (b)) and a negative correlation between the misalignment β and the ratio μ/L (figures 9(c) and (d)).The distribution of misalignments measured by analyzing orientation distributions for AMB-1 cells is peaked between 5° and 7° with an average misalignment of 6.5° (figure 9(d)).

5. Discussion

For each AMB-1 cell we studied, we observed that the relationship between the apparent cell orientation in the focal plane, θ, and the cell rotation around its own long axis, ϕ, follows the form predicted for a cell rotating around an axis slightly different from its cell body axis and exactly aligned with the direction of the magnetic field (equation (11)). This clearly demonstrates that there is a small permanent misalignment between cell body axis and magnetic moment in cells of AMB-1. The fact that this misalignment is not affected by the strength of the magnetic field indicates that the potential effect of the susceptibility anisotropy of the magnetosome chain is negligible for cells of AMB-1 at the field strengths employed.

The method presented here to detect and to precisely measure the angle between magnetic moment and cell body axis relies on the analysis of movies recorded with phase contrast microscopy. The relative loss of accuracy due to low-resolution imaging (the

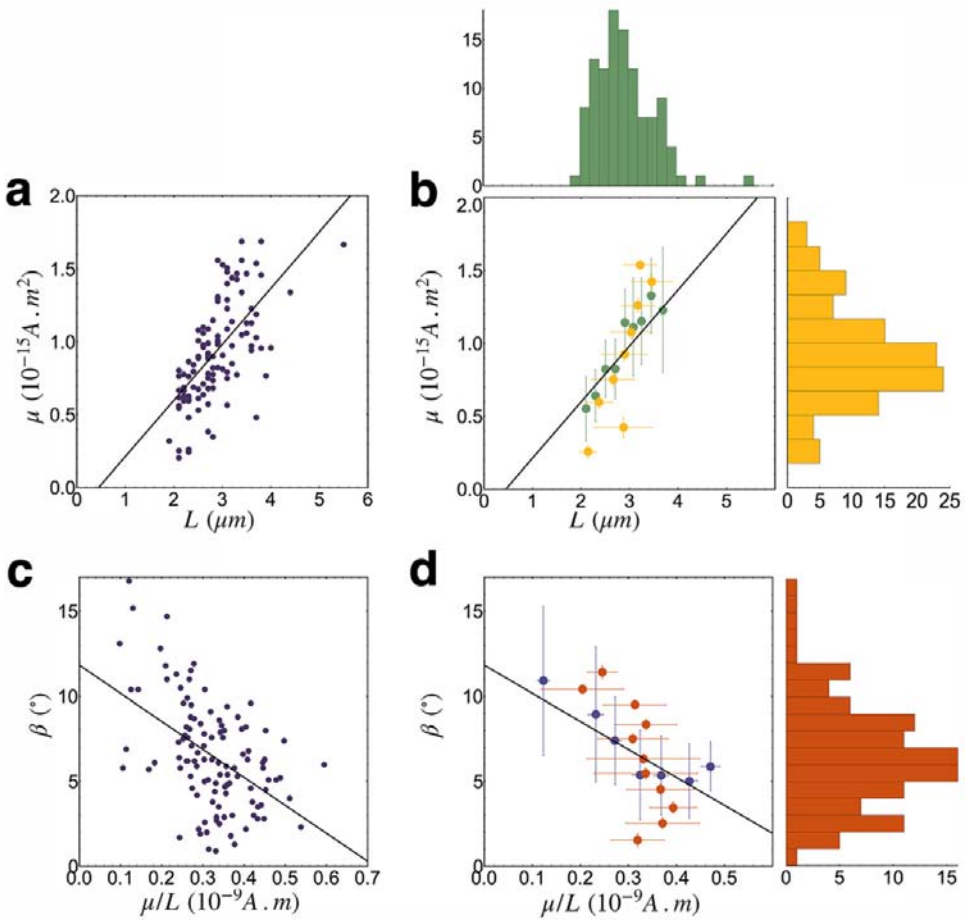

Figure 9. Summary of results for all 111 studied cells of *Magnetospirillum magneticum* strain AMB-1. (a) Relationship between L and μ. The Pearson correlation coefficient is $PCC = 0.7$. The black line is a linear fit to the data ($\mu = aL - b$, with $a = 3.8 \times 10^{-10}$ A · m and $b = 1.7 \times 10^{-16}$ A · m^2). (b) Same plot as in (a), with the data binned either according to the value of L (green symbols) or μ (yellow symbols). Only bins containing more than 3 cells were included. Error bars correspond the standard deviation of the values of L of μ for the cells in the bin. The corresponding distributions of cell length and magnetic moment are shown above and on the right of the plot, respectively. (c) Relationship between β and μ/L. $PCC = -0.5$ and the solid black line is a linear fit to the data ($\beta = -a\mu/L + b$, with $a = 1.6 \times 10^{16}$ ° · A^{-1} · m^{-1} and $b = 12°$). (d) Same plot as in (c), with the data binned either according to the value of μ/L (dark blue symbols) or β (red symbols). Only bins containing more than 3 cells were included. Error bars correspond the standard deviation of the values of μ/L of β for the cells in the bin. The corresponding distribution of misalignments is shown on the right of the plot. The mean value of β for this cell population was 6.5° with a standard deviation of 3.2°.

orientation of the cell in the focal plane, θ, is measured with a precision of only 3°) is compensated by the acquisition of a large number of frames for each cell (minimum 1500 frames per cell). By using non-motile cells, we eliminate any effect due to the active rotation of the flagella and only have to consider the magnetic torque and the thermal motions in our analysis. Fitting the distribution of orientations of a cell (with equation (11)) leads to an effective measurement of β, the misalignment between $\vec{\mu}$ and $\vec{L}$, with a precision better than 0.5°.

There may be a number of explanations for the magnetic moment misalignment we observed in cells of AMB-1. First, the rigid MamK protein filament to which the magnetosomes are attached may not always be perfectly aligned with the cell axis, thus the axis of the magnetosome chain is likely to have a small inclination with respect to the cell axis—something we indeed observed using TEM. Second, Orue and coworkers showed that in *Magnetospirillum gryphiswaldense* strain MSR-1 the magnetic moments of individual magnetosomes are not aligned, and instead are found at an angle of approximately 20° from the axis of the magnetosome chain, while the chain itself adopts a helical shape [23]. Since AMB-1 and MSR-1 are morphologically similar, the same behaviour can be expected in AMB-1. Although Orue and colleagues find the total magnetic moment to be still roughly parallel to the magnetosome chain axis [23], their findings challenge the simple assumption of a linear magnetosome chain aligned with the cell axis, and help understand how small misalignments between cell axis and magnetic moment might arise.

This work is to our knowledge the first to report and measure the misalignment between cell axis and magnetic dipole moment in members of the genus *Magnetospirillum*. This could be because most studies that involve tracking of MTB cells in a magnetic field are performed on live bacteria, and the fast rotation of the cell complicates the detection of the misalignment.

Yet, this phenomenon is significant since the distribution of misalignments recorded has a mean of 6.5°, with a significant number of cells having a misalignment higher than 10° (figures 9(c) and (d)). And although measurements presented here were done for a single species of *Magnetospirillum*, it is likely that all species of MTB exhibit some degree of misalignment between the direction of their magnetic moment and their swimming direction, especially in spherical species such as cocci which lack a clear morphological axis, or in large multicellular species, where the precise alignment of the magnetic moment with the propulsion axis might be more difficult to achieve.

Importantly, the method presented here provides a way to correct the misalignment in order to recover non-biased orientation distributions for the cell magnetic axis, from which the magnetic moment of individual MTB can be measured. This method is based on a direct fitting of the corrected orientation distributions, with only two external parameters: the magnetic field strength and the absolute temperature, two easily measurable quantities. Figure 8 presents data measured at two different field strengths on the same cell. Before correction, there is a significant (20%) difference between the magnetic moments measured for that cell at different fields ($\mu = 3.5 \times 10^{-16}$ and $\mu = 2.9 \times 10^{-16}$ A · m^2 at respectively 1.0 and 1.9 mT). In contrast, after correction the estimated values ($\mu = 10 \times 10^{-16}$ and $\mu = 9.0 \times 10^{-16}$ A · m^2) are within 10% of each other (which corresponds to the error we estimate for this measurement). Most importantly, there is a 3-fold difference between the values obtained before and after correction. This demonstrates that a 6° misalignment is sufficient to significantly alter the measurement of μ made from the analysis of the orientation distribution.

After misalignment correction, the remanent magnetic moment measured for this cell population is $\mu = (9.5 \pm 3.7) \times 10^{-16}$ (mean ± st. dev.), in excellent agreement with the estimate obtained by TEM for the same population ($\mu = 10.2 \pm 3.4 \times 10^{-16}$). The 20° tilt in the magnetic moment of individual magnetosomes with respect to the chain axis observed in MSR-1 [23] could also be present in AMB-1 and would further reduce the overall magnetic moment by a factor $\cos(20°) = 0.93$ compared to the estimated saturation moment. We note that the average magnetic moment measured here is larger than the one we previously reported using the same method for the same MTB species [27]. It is also above typical values reported for AMB-1 by other groups ($\mu = 1.0 \times 10^{-16}$ A · m^2 from iron uptake [47], $\mu = 0.5 \times 10^{-16}$ A · m^2 from optical magnetic imaging [48], $\mu = 0.7 \times 10^{-16}$ A · m^2 from vibrating sample magnetometry [49], $\mu = 0.9 - 7.1 \times 10^{-16}$ A · m^2 from a variety of other techniques [27]). These differences can be explained by differences in culturing, but also by the fact that since our method is based on single-cell measurements, only cells that exhibit a magnetic response were studied. In conclusion, our work shows that correcting for the misalignment between body axis and magnetic moment is crucial when analyzing orientation distributions of MTB, and calls for a reassessment of measurements of magnetic moments based on statistical analysis of cell orientations. It shows that the effect of misalignment can be corrected for in such measurements, at least for dead cells, allowing the precise measurement of the magnetic moment of individual cells.

Another interesting aspect of the single cell measurements presented here is that they clearly show that μ increases with L (figures 9(a) and (b)). This suggests that after cellular division (the cell length is then about 2 μm and the magnetic moment around 0.6×10^{-15}), the cell and the magnetosome chain grow concurrently until the cell has doubled in length (reaching $L \simeq 4$ μm) and the magnetic moment has doubled in magnitude (reaching $\mu \simeq 1.3 \times 10^{-15}$). These numbers further suggest that during cellular division the magnetosome chain is split more or less equally between the two daughter cells. We see no evidence that longer cells limit their magnetosome production at any point to the strict minimum required to align with an external magnetic field. In addition, although β does not clearly correlate with either L or μ ($PCC = 0.03$ and $PCC = -0.34$ respectively), it is negatively correlated with μ/L ($PCC = -0.5$). This relationship might be explained by the fact that, for a given L, higher values of μ mean longer and/or more linear magnetosome chains, thus limiting the magnitude of a possible misalignment.

A misalignment between the cell's magnetic moment and propulsion axis will complicate the swimming motion of individual cells [18, 20, 50]. To swim, MTB rotate their flagella, which in turn may force the cell body to rotate. A natural assumption is that the rotation axis corresponds to the cell axis. But if a misalignment exists between magnetic moment and cell body axis, the rotation around the cell axis creates a misalignment between the magnetic moment and the field, which is unfavorable at high fields. In the presence of both a misalignment between magnetic moment and cell body axis and a magnetic field, one expects a motion which is the superposition of two helical motions, one high-frequency helical motion due to flagellar rotation and another lower frequency helical motion due to the precession of the propulsion axis (determined by the cell body axis and flagellar position) around the rotation axis (determined at high field by the magnetic moment) [18, 20]. Indeed, helical trajectories are commonly observed for MTB species [24]. They have been well documented in particular for cocci such as MO-1 [30] and MYC-1 [18] and for magnetotactic multicellular prokaryotes [21, 29]. They have been also reported for *Magnetospirillum* species [19]. Since each cell is characterized by a specific magnetic moment and a specific misalignment, swimming trajectories need to be studied at the single cell level. This could be an important consideration for the analysis of cell collective motions and biotechnology applications.

Acknowledgments

This work was funded by the Natural Sceince and Engineering Research Council of Canada.

ORCID iDs

Cécile Fradin https://orcid.org/0000-0001-8329-4953

References

[1] Bellini S 2009 On a unique behavior of freshwater bacteria *Chin. J. Oceanol. Limnol.* **27** 3–5
[2] Blakemore R 1975 Magnetotactic bacteria *Science* **190** 377–9
[3] Blakemore R P 1982 Magnetotactic bacteria *Annu. Rev. Microbiol.* **36** 217–38
[4] Uebe R and Schüler D 2016 Magnetosome biogenesis in magnetotactic bacteria *Nat. Rev. Microbiol.* **14** 621
[5] Frankel R B, Bazylinski D A, Johnson M S and Taylor B L 1997 Magneto-aerotaxis in marine coccoid bacteria *Biophys. J.* **73** 994–1000
[6] Lefèvre C T, Bennet M, Landau L, Vach P, Pignol D, Bazylinski D A, Frankel R B, Klumpp S and Faivre D 2014 Diversity of magneto-aerotactic behaviors and oxygen sensing mechanisms in cultured magnetotactic bacteria *Biophys. J.* **107** 527–38
[7] Maratea D and Blakemore R 1981 Aquaspirillum magnetotacticum sp. nov., a magnetic spirillum *Int. J. Systematic Evolutionary Microbiol.* **31** 452–5
[8] Schleifer K H, Schüler D, Spring S, Weizenegger M, Amann R, Ludwig W and Köhler M 1991 The genus *Magnetospirillum* gen. nov. description of *Magnetospirillum* gryphiswaldense sp. nov. and transfer of aquaspirillum magnetotacticum to *Magnetospirillum* magnetotacticum comb. nov. *Systematic Appl. Microbiol.* **14** 379–85
[9] Matsunaga T, Sakaguchi T and Tadakoro F 1991 Magnetite formation by a magnetic bacterium capable of growing aerobically *Appl. Microbiol. Biotechnol.* **35** 651–5
[10] Balkwill D, Maratea D and Blakemore R 1980 Ultrastructure of a magnetotactic spirillum *J. Bacteriol.* **141** 1399–408
[11] Arakaki A, Webb J and Matsunaga T 2002 A novel protein tightly bound to bacterial magnetic particles in *Magnetospirillum magneticum* strain AMB-1 *J. Biol. Chem.* **278** 8745–50
[12] Komeili A, Li Z, Newman D K and Jensen G J 2006 Magnetosomes are cell membrane invaginations organized by the actin-like protein mamk *Science* **311** 242–5
[13] Scheffel A, Gruska M, Faivre D, Linaroudis A, Plitzko J M and Schüler D 2006 An acidic protein aligns magnetosomes along a filamentous structure in magnetotactic bacteria *Nature* **440** 110
[14] Draper O, Byrne M E, Li Z, Keyhani S, Barrozo J C, Jensen G and Komeili A 2011 Mamk, a bacterial actin, forms dynamic filaments *in vivo* that are regulated by the acidic proteins MAMJ and LIMJ *Mol. Microbiol.* **82** 342–54
[15] Frankel R B and Blakemore R 1980 Navigational compass in magnetic bacteria *J. Magn. Magn. Mater.* **15** 1562
[16] Bazylinski D A, Garratt-Reed A J and Frankel R B 1994 Electron microscopic studies of magnetosomes in magnetotactic bacteria *Microsc. Res. Tech.* **27** 389–401
[17] Lefèvre C T and Bazylinski D A 2013 Ecology, diversity, and evolution of magnetotactic bacteria *Microbiol. Mol. Biol. Rev.* **77** 497–526
[18] Pan Y, Lin W, Li J, Wu W, Tian L, Deng C, Liu Q, Zhu R, Winklhofer M and Petersen N 2009 Reduced efficiency of magnetotaxis in magnetotactic coccoid bacteria in higher than geomagnetic fields *Biophys. J.* **97** 986–91
[19] Zhu K *et al* 2010 Isolation and characterization of a marine magnetotactic spirillum axenic culture qh-2 from an intertidal zone of the china sea *Res. Microbiol.* **161** 276–83
[20] Yang C, Chen C, Ma Q, Wu L and Song T 2012 Dynamic model and motion mechanism of magnetotactic bacteria with two lateral flagellar bundles *J. Bionic Eng.* **9** 200–10
[21] Almeida F P, Viana N B, Lins U, Farina M and Keim C N 2013 Swimming behaviour of the multicellular magnetotactic prokaryote '*Candidatus* Magnetoglobus multicellularis' Under applied magnetic fields and ultraviolet light *Antonie Leeuwenhoek* **103** 845–57
[22] Faivre D and Schuler D 2008 Magnetotactic bacteria and magnetosomes *Chem. Rev.* **108** 4875–98
[23] Orue I *et al* 2018 Configuration of the magnetosome chain: a natural magnetic nanoarchitecture *Nanoscale* **10** 7407–19
[24] Esquivel D M S and Lins De Barros H G 1986 Motion of magnetotactic microorganisms *J. Exp. Biol.* **121** 153–63
[25] Ērglis K, Wen Q, Ose V, Zeltins A, Sharipo A, Janmey P A and Cēbers A 2007 Dynamics of magnetotactic bacteria in a rotating magnetic field *Biophys. J.* **93** 1402–12
[26] Penninga I, de Waard H, Moskowitz B M, Bazylinski D A and Frankel R B 1995 Remanence measurements on individual magnetotactic bacteria using a pulsed magnetic field *J. Magn. Magn. Mater.* **149** 279–86
[27] Nadkarni R, Barkley S and Fradin C 2013 A comparison of methods to measure the magnetic moment of magnetotactic bacteria through analysis of their trajectories in external magnetic fields *PLoS One* **8** e82064
[28] Zhu X, Ge X, Li N, Wu L-F, Luo C, Ouyang Q, Tu Y and Chen G 2014 Angle sensing in magnetotaxis of *Magnetospirillum magneticum* amb-1 *Integr. Biol.* **6** 706–13
[29] Lins U and Farina M 1999 Organization of cells in magnetotactic multicellular aggregates *Microbiol. Res.* **154** 9–13
[30] Lefèvre C T, Bernadac A, Yu-Zhang K, Pradel N and Wu L-F 2009 Isolation and characterization of a magnetotactic bacterial culture from the mediterranean sea *Environ. Microbiol.* **11** 1646–57
[31] Kalmijn A 1981 Biophysics of geomagnetic field detection *IEEE Trans. Magn.* **17** 1113–24
[32] Lemaire B, Davidson P, Ferré J, Jamet J, Panine P, Dozov I and Jolivet J 2002 Outstanding magnetic properties of nematic suspensions of goethite (α-feooh) nanorods *Phys. Rev. Lett.* **88** 125507
[33] Wolin E, Wolin M and Wolfe R 1963 Formation of methane by bacterial extracts *J. Biol. Chem.* **238** 2882–6
[34] Bazylinski D A, Dean A J, Schüler D, Phillips E J and Lovley D R 2000 N2-dependent growth and nitrogenase activity in the metal-metabolizing bacteria, geobacter and magnetospirillum species *Environ. Microbiol.* **2** 266–73
[35] Le Nagard L, Morillo-López V, Fradin C and Bazylinski D A 2018 Growing magnetotactic bacteria of the genus *Magnetospirillum*: strains MSR-1, AMB-1 and MS-1 *J. Vis. Exp.* e58536
[36] Constantino M A, Jabbarzadeh M, Fu H C and Bansil R 2016 Helical and rod-shaped bacteria swim in helical trajectories with little additional propulsion from helical shape *Sci. Adv.* **2** e1601661
[37] Hitchcock A P 2018 aXis2000 is written in interactive data language (IDL) and is available free for non-commercial use from (http://unicorn.mcmaster.ca/aXis2000.html)
[38] Goering E, Lafkioti M, Gold S and Schuetz G 2007 Absorption spectroscopy and xmcd at the verwey transition of Fe_3O_4 *J. Magn. Magn. Mater.* **310** e249–51
[39] Zahn C, Keller S, Toro-Nahuelpan M, Dorscht P, Gross W, Laumann M, Gekle S, Zimmermann W, Schüler D and Kress H 2017 Measurement of the magnetic moment of single magnetospirillum gryphiswaldense cells by magnetic tweezers *Sci. Rep.* **7** 3558
[40] Haynes W M 2014 *CRC Handbook of Chemistry and Physics* (Boca Raton, FL: CRC Press)
[41] Moskowitz B, Frankel R B, Flanders P, Blakemore R and Schwartz B B 1988 Magnetic properties of magnetotactic bacteria *J. Magn. Magn. Mater.* **73** 273–88

[42] Rosenblatt C, de Araujo F F T and Frankel R B 1982 Light scattering determination of magnetic moments of magnetotactic bacteria *J. Appl. Phys.* **53** 2727–9
[43] Huízar-Félix A, Muñoz D, Orue I, Magén C, Ibarra A, Barandiarán J, Muela A and Fdez-Gubieda M 2016 Assemblies of magnetite nanoparticles extracted from magnetotactic bacteria: a magnetic study *Appl. Phys. Lett.* **108** 063109
[44] Dunin-Borkowski R E, McCartney M R, Frankel R B, Bazylinski D A, Pósfai M and Buseck P R 1998 Magnetic microstructure of magnetotactic bacteria by electron holography *Science* **282** 1868–70
[45] Dunin-Borkowski R E, McCartney M R, Pósfai M, Frankel R B, Bazylinski D A and Buseck P R 2001 Off-axis electron holography of magnetotactic bacteria: magnetic microstructure of strains mv-1 and ms-1 *Eur. J. Mineral.* **13** 671–84
[46] Kalirai S S, Bazylinski D A and Hitchcock A P 2013 Anomalous magnetic orientations of magnetosome chains in a magnetotactic bacterium: magnetovibrio blakemorei strain mv-1 *PLoS One* **8** e53368
[47] Smith M, Sheehan P, Perry L, O'Connor K, Csonka L, Applegate B and Whitman L 2006 Quantifying the magnetic advantage in magnetotaxis *Biophys. J.* **91** 1098–107
[48] Le Sage D, Arai K, Glenn D, DeVience S, Pham L, Rahn-Lee L, Lukin M, Yacoby A, Komeili A and Walsworth R 2013 Optical magnetic imaging of living cells *Nature* **496** 486
[49] Krichevsky A, Smith M, Whitman L, Johnson M, Clinton T, Perry L, Applegate B, O'Connor K and Csonka L 2007 Trapping motile magnetotactic bacteria with a magnetic recording head *J. Appl. Phys.* **101** 014701
[50] Nogueira F S and Lins de Barros H G 1995 Study of the motion of magnetotactic bacteria *Eur. Biophys. J.* **24** 13–21